

Wrinkling of 3D auxetic bilayers in tension

Sairam Pamulaparthy Venkata^{*†}, Valentina Balbi, and Michel Destrade
*School of Mathematical and Statistical Sciences,
 University of Galway, H91 TK33 Galway, Ireland*

Yuxin Fu[†]
*Department of Mechanics,
 Tianjin University, Tianjin 300072, China*

Hooman Danesh
*Institute of Applied Mechanics,
 RWTH Aachen University,
 Mies-van-der-Rohe-Str.1, 52074, Aachen, Germany*

Yibin Fu
*School of Computer Science and Mathematics,
 Keele University, Keele,
 Staffordshire ST5 5BG, United Kingdom*

^{*}Contact author: S.PamulaparthyVenkata1@universityofgalway.ie

[†]These authors contributed equally to this work.

Bilayers (soft substrates coated with stiff films) are commonly found in nature with examples including skin tissue, vesicles, or organ membranes. They exhibit various types of instabilities when subjected to compression, depending on the contrast in material properties between the two components. In this letter, we unravel the mechanisms behind wrinkling instabilities in *auxetic* bilayer systems under uni-axial *tension*. We find that in tension, a soft bilayer can experience large lateral contraction. With an adequate contrast in the Poisson ratios, compressive stresses may develop and generate wrinkles aligned with the tensile direction. We model analytically the onset of wrinkles and develop a new numerical method to validate our predictions with advanced Finite Element simulations in ABAQUS. Our findings reveal that wrinkles are observed when the Poisson ratio of the substrate is greater than that of the film. As the two Poisson ratios converge to a common value, the critical stretch of instability shoots up rapidly, and the wrinkling disappears. We also confirm these results by asymptotic analysis. Our proposed numerical method is versatile and can be used to predict wrinkling in bilayers where auxeticity is associated with microstructural patterns. Using inverse analysis, we design the film microstructures to achieve desired effective Poisson's ratios and further validate the effective properties of these microstructures with the Finite Element code, FEAP. We show that the critical stretch ratio for buckling in auxetic structures with microstructural patterns is in strong agreement with the predictions of homogenized models. The new method proposed in this letter has a significant potential for controlling surface patterns of auxetic skin grafts and hydrogel organ patches under mechanical loads. Moreover, the asymptotic expressions in this work can be used under finite strain for buckling-based metrology applications.

Auxetics, materials with negative Poisson's ratio, expand in all directions under uni-axial tension. For 3D isotropic materials with auxetic behavior, the theoretical value of Poisson's ratio ranges between -1 and 0.5 [1]. Thanks to rapid advancement in additive and subtractive manufacturing techniques [2, 3], along with extensive research on negative Poisson ratio materials, auxetics have shown promising applications in various fields [4–9].

Compliant substrates coated with thin-layered stiff films (bilayers) are commonly found in nature; for example, skin tissue consists of a thin, stiff epidermal layer attached to a thick, soft dermis. When subject to mechanical loads, bilayer systems can exhibit surface patterns through wrinkles. This instability phenomenon has found a broad range of applications, in optical sensors [10], novel flexible electronics [11–13], tunable phase gratings [14], buckling-based metrology [15, 16], surface wetting [17], and for buckling-related applications in soft matter [18].

The formation of these surface patterns is controlled by different parameters, such as the contrast in mate-

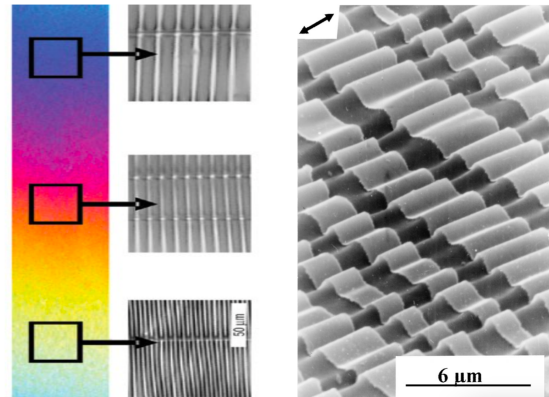


Figure 1. Left: Optical micrograph of a Polystyrene film on a silicon substrate taken from Stafford *et al.* [15]. After stretching the film wrinkles with different wavelength depending on the thickness of the film (decreasing from top to bottom insets). Right: Scanning Electron Microscope imaging of a natural rubber substrate coated with a gold film, when elongated (arrow) to 50% strain [19].

rial properties [20, 21], differential growth [22], film-to-substrate thickness ratio [23, 24], initial imperfections [25], substrate nonlinearity [26, 27], interfacial mechanics [28, 29], etc.

A survey of the literature shows that wrinkles appearing in tension are seldom studied beyond the linear-elastic framework [30], although they have been established experimentally under large strains [15, 19], see Figure 1.

In this letter, we unravel the wrinkling instabilities of auxetic bilayers made of a thin stiff film bonded to a compliant substrate undergoing large *tension*. Under a uniaxial tension applied along the X-direction, such bilayers is expected to eventually develop wrinkles aligned with that direction, as shown in Figure 1 (right), provided compressive stresses develop along the Y-direction because of a sufficient Poisson ratio contrast. We discover that wrinkles are generated in bilayers subjected to uni-axial tension only when the Poisson ratio of the substrate is greater than that of the film. Moreover, we devise a new approach which uses a combination of semi-analytical and numerical methods to predict the wrinkling pattern of the bilayer in tension. This approach allows us to establish that wrinkles disappear when the Poisson ratios of film and substrate converge to a common value. Typically, the wavelength of wrinkles increases as the Poisson's ratios of the film and substrate approach each other and decreases as they diverge. However, when the film and substrate are highly compressible ($\nu_f = -0.95$ and $\nu_s < -0.7$), this trend reverses, and the wavelength decreases, as illustrated in Figure 3(d).

We also derive asymptotic expressions for critical stretch ratios and critical wavenumbers. These new expressions are valid in finite strains and useful for buckling-based metrology applications. Finally, we employ an inverse design approach to achieve a desired effective Poisson's ratio in the film by altering its microstructure. This method can be applied to the manufacturing of skin grafts, where the graft's microstructure is chosen to avoid undesired wrinkling.

We start by implementing Finite Element simulations of a bilayer in tension in ABAQUS [31](see Supplementary material: Numerical model). We model the mechanical behaviour of each layer with the Blatz–Ko strain energy function [32] in the following form:

$$W = c_1(I_1 - 3 + (I_3^{-\beta} - 1)/\beta) + c_2(I_2/I_3 - 3 + (I_3^\beta - 1)/\beta), \quad (1)$$

where $c_1 = \alpha \frac{\mu}{2}$, $c_2 = (1 - \alpha) \frac{\mu}{2}$, $\beta = \frac{\nu}{1-2\nu}$, \mathbf{F} is the deformation gradient and $I_1 = \text{tr}(\mathbf{F}\mathbf{F}^T)$, $I_2 = I_3 \text{tr}[(\mathbf{F}\mathbf{F}^T)^{-1}]$, $I_3 = \det(\mathbf{F}\mathbf{F}^T)$ are the principal invariants of $\mathbf{B} = \mathbf{F}\mathbf{F}^T$. The material constants are the non-dimensional parameter $0 < \alpha < 1$, the initial shear modulus $\mu > 0$, and the Poisson ratio $-1 < \nu \leq 1/2$.

Auxetic materials are highly compressible due to their negative Poisson ratio (thus far away from the incompressibility limit of a Poisson ratio equal to 1/2). Blatz–Ko strain energy functions with a negative Poisson ratio can thus be used to model auxetics, although with certain limitations [33]. For example, Ciambella and Saccomandi [35] use the Blatz–Ko strain energy to capture the

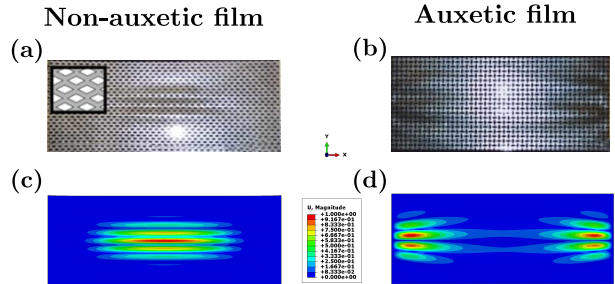


Figure 2. Thin acetate sheets (top) under uni-axial tension, with (a) non-auxetic micro-structural patterns and (b) auxetic micro-structural patterns [34]. For conventional sheets, wrinkles develop at the center of the sheet. For auxetic sheets, they appear near the clamped edges. Corresponding buckling profiles (bottom) obtained in ABAQUS with the Blatz–Ko model in Equation (1). Here $\alpha = 0.4$, $\mu = 0.53$ GPa, and $\nu = 0.38, -0.2$ in (c) and (d), respectively.

experiments of Choi and Lakes [36] on auxetic materials. The model is also adequate to capture the experimental behaviors of membranes (no substrate) under tension, from auxetic to conventional Poisson ratios, see Figure 2. We thus implement a custom-made material subroutine in ABAQUS for the energy in Equation (1) and use it to model the mechanical behavior of the two layers. To induce the wrinkling pattern in the bi-layer under tension, we write a custom-made python script which implements periodic boundary conditions as shown in Figure 3(a) (see the section Finite Element Simulations in the Supplementary Material for further details on the numerical model).

Now, using the linear buckling analysis in ABAQUS, we find that the bilayer in tension develops wrinkles only when the Poisson ratio of the film (ν_f) is smaller than that of the substrate (ν_s), as summarised in Figure 3 (b). This result recovers the predictions obtained by Nikravesch *et al.* [37] for linear-elastic bilayer systems.

To predict the critical stretch and wavenumber of the wrinkling instability, we perform a linear stability analysis (see the section Semi-analytical Method in the Supplementary Material). We first calculate the base elastic solution. We then add a small incremental deformation to perturb the base solution and derive the associated incremental problem. Finally, we numerically solve the incremental problem in Mathematica [38] and find the critical stretch and wavenumber for the onset of wrinkling. To illustrate our results, we fix the Poisson ratio of the bilayer while varying that of the film, and vice versa. In Figure 3(c), we plot the critical stretch λ_c and the corresponding wrinkling wavenumber k_c against ν_f for a bilayer with a quasi-incompressible substrate. When the substrate is quasi-incompressible ($\nu_s = 0.495$) and the film's Poisson ratio ranges in $\nu_f \in (-0.95, 0.495)$, we observe wrinkles. Here the Poisson ratio of the substrate is greater than that of film, and under uniaxial tension, the film expands more than the substrate along the Z-direction, resulting in compressive stresses and the formation of wrinkles parallel to the X-direction. We observe that the critical stretch ratio values predicted from the semi-analytical analysis (Mathematica) and the FE buckling analysis (ABAQUS) match well, as long as

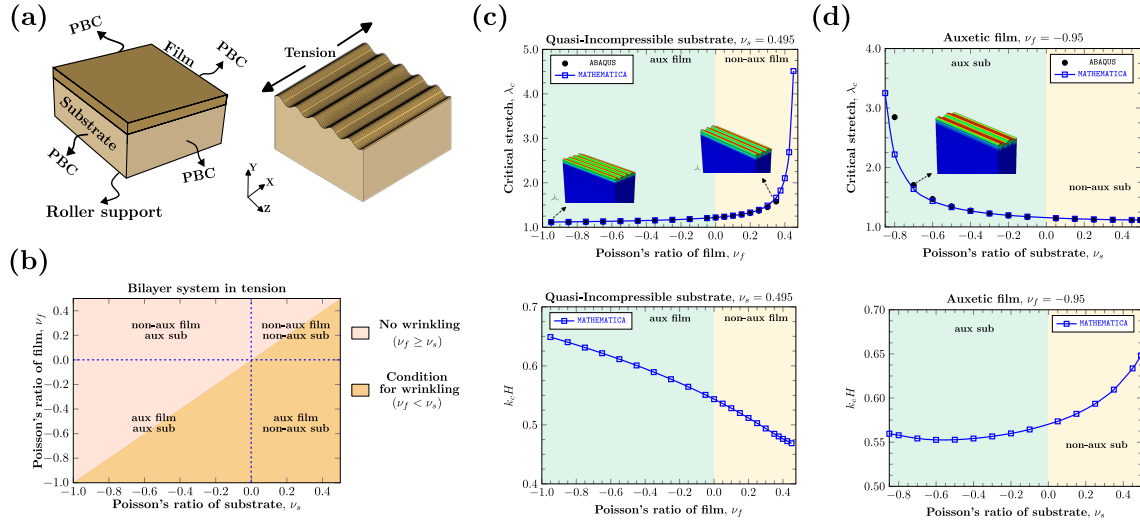


Figure 3. (a) Our model of a bilayer system with periodic boundary conditions. The system is infinite in the X- and Z-directions and is stretched along the X-direction. Our numerical results show that wrinkles develop parallel to the X-direction, provided there is enough contrast between the mechanical parameters of the materials. (b) Wrinkling condition according to the contrast between the Poisson ratios of film and substrate. (c-d) Critical stretch λ_c for wrinkling and corresponding non-dimensional critical wavenumber $k_c H$ plotted against the Poisson ratio of one layer (k_c is the critical wavenumber and H is the film initial thickness). In (c) the substrate is quasi-incompressible ($\nu_s = 0.495$) and in (d) the film is highly auxetic ($\nu_f = -0.95$).

$\nu_f \leq 0.35$. Beyond this value, ABAQUS ceases to predict wrinkles in the desired direction and gives negative eigenvalues, suggesting the load direction has to be reversed to obtain wrinkles, which is unphysical. An auxetic film ($\nu_f < 0$) expands in all directions under tension while the incompressible substrate contracts along the Z direction, leading to a compressive stress in the film. Hence only low values of the critical stretch are required for the wrinkles to occur. As the Poisson ratio of the film increases and moves closer to that of the substrate, the values of the critical stretch shoot up sharply, supporting our findings in Figure 3(b).

We also observe wrinkles when we take the film to be highly auxetic (with Poisson ratio $\nu_f = -0.95$) and the substrate Poisson ratio varies in $\nu_s \in (-0.95, 0.495]$. Figure 3(d) shows how λ_c and k_c vary with ν_s for a bilayer with a highly auxetic film. Again, we find good

agreement between theory and simulations for a certain range, when $-0.7 \leq \nu_s \leq 0.495$. For $\nu_s < -0.8$, ABAQUS stops providing meaningful predictions. In both scenarios, wrinkles occur at low stretching values ($\lambda_c < 1.5$), except as $\nu_s \rightarrow \nu_f$. In this limit, the critical stretch increases dramatically because both film and substrate experience the same transverse contraction so that no compressive stress nor wrinkles develop. Similarly to Figure 3(c), Figure 3(d) shows that the higher the Poisson ratio contrast is, the larger the wavelength of the wrinkles.

In summary, we found that to ensure early wrinkling in tension, a large contrast in Poisson's ratio is required, for example by taking one material to be auxetic and the other non-auxetic.

Analytical expressions for bilayers under uni-axial tension have historically been derived only for linear elastic materials, as seen in the works of Volynskii *et al.* [19], Chung *et al.* [39], and Nikravesht *et al.* [37]. The critical strain and wavenumber expressions are given by:

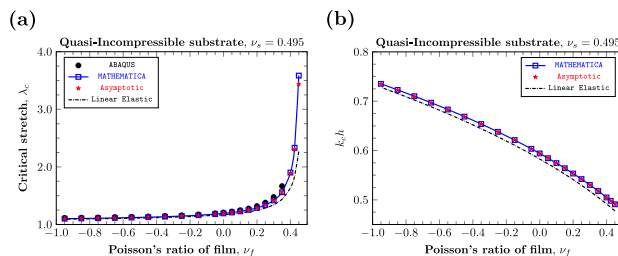


Figure 4. Comparison between our asymptotic results (red star markers), linear asymptotic results (dashed lines), numerical simulations (black squares) and linear stability analysis (empty blue squares). Both substrate and film are neo-Hookean ($\alpha_s = \alpha_f = 1$ in Equation (1)) and the substrate is quasi-incompressible ($\nu_s = 0.495$). (a-b): Critical stretch λ_c and corresponding critical wavenumber $k_c h$ against the Poisson ratio of film ν_f . The asymptotic equations for the linear case are reported in Equation 2.

$$\varepsilon_c = \frac{1}{4(\nu_s - \nu_f)} \left(3 \frac{\mu_s}{\mu_f} \frac{1 - \nu_f}{1 - \nu_s} \right)^{2/3},$$

$$k_c h = \left(3 \frac{\mu_s}{\mu_f} \frac{1 - \nu_f}{1 - \nu_s} \right)^{1/3}, \quad (2)$$

Here, h is the current thickness of the film. These expressions, valid under the plane-strain approximation and at low strains ($\ll 10\%$), have been applied in buckling-based metrology to determine the Young's modulus of the film [15].

However, for a bilayer system under uni-axial tension the plane-strain assumption is not valid. To address this, we employ asymptotic analysis to derive the expressions for λ_c and $k_c h$ based on the material properties of film and substrate layers, in finite strain deformation. To de-

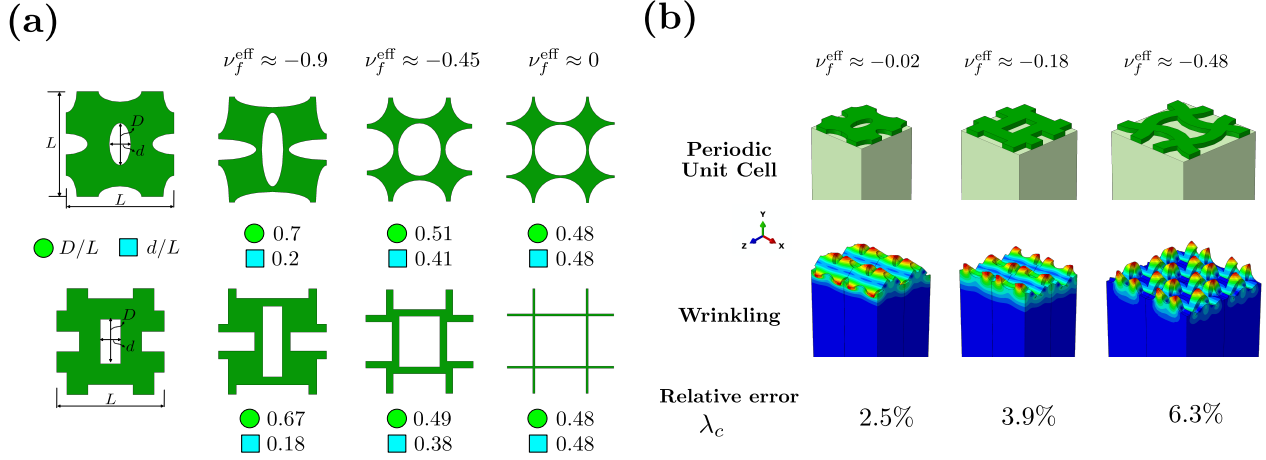


Figure 5. (a) Influence of microstructural geometry on the effective Poisson's ratio (ν_f^{eff}) in auxetic films with orthogonal-oval and rectangular-void patterns. Films with desired effective Poisson's ratios are obtained using inverse analysis. (b) Comparison of undeformed and deformed configurations in bilayers with distinct auxetic microstructures, each designed to achieve specific Poisson's ratio in the small strain regime. Film and substrate base materials exhibit compressible ($\nu_f = 0.1$) and nearly incompressible ($\nu_f = 0.495$) properties, respectively. Periodic boundary conditions are applied on the lateral faces of the domain along X and Z and the system is subjected to uni-axial tension along X. We observe that the wrinkles are generated parallel to the direction of tension. The bottom of (b) shows the percentage relative error in critical stretch between homogenized bilayers (Figure 3(c)) and those with microstructural patterns, obtained in ABAQUS with the Blatz–Ko model.

rive universal asymptotic expansions in large deformations for the critical strain and wavenumber, we follow Cai and Fu [40, 41]. For simplicity, we take $\alpha_s = \alpha_f = 1$ in Equation (1) and assume that the shear modulus ratio $r = \mu_s/\mu_f$ is of order $(k_c h)^3$. We find the following asymptotic expressions:

$$\lambda_c = 1 + \frac{[(1 - \nu_f)(1 - \nu_s)]^{2/3}}{(\nu_s - \nu_f)(8\nu_s/3 - 2)^{2/3}} r^{2/3} + \frac{(1 - \nu_f)(2\nu_s - 1)}{(\nu_s - \nu_f)(4\nu_s - 3)} r + c_4 r^{4/3} + c_5 r^{5/3} + c_6 r^2 + \mathcal{O}(r^{7/3}), \quad (3)$$

and

$$k_c h = \left[\frac{4(1 - \nu_f)(1 - \nu_s)}{1 - 4\nu_s/3} \right]^{1/3} r^{1/3} + d_3 r + d_4 r^{4/3} + d_5 r^{5/3} + \mathcal{O}(r^2), \quad (4)$$

where the coefficients $c_4, \dots, c_6, d_3, \dots, d_5$ are shown in the section Asymptotic Analysis in the Supplementary Material. We find that in small deformations our predictions recover the linear-elastic behavior, as described in Equation (2). However, as $\nu_f \rightarrow \nu_s$, the critical strain becomes large and the linear-elastic results greatly underestimate the numerical results, while our asymptotic expressions in Equations (3) and (4) give good agreement. Figure 4(a) and (b) show how λ_c and $k_c h$ vary with ν_f when $\nu_s = 0.495$ (quasi-incompressible substrate). In Figure S.2 (Supplementary Material), we plot the variations of λ_c and $k_c h$ with the Poisson ratio of the film ($0 < \nu_f < 0.45$) for different values of shear moduli contrast μ_f/μ_s using Equations 3-4.

We now demonstrate how our results can be used to predict wrinkling instabilities in materials with auxetic patterns. Indeed, auxetic properties can be obtained at

a continuum level with a careful design of holes or voids at the micro-scale [6, 42]. Figure 5(a) illustrates how the geometric parameters of the orthogonal oval and rectangular voids generate the effective Poisson's ratios (ν_f^{eff}). Using the inverse design approach outlined by Danesh *et al.* [43], we generate the geometries for a set of auxetic structures with the desired effective Poisson's ratios (ν_f^{eff}) in the small strain regime, as depicted in Figure 5(b). We validate the effective properties of these resulting geometries with the Finite Element code, FEAP [44], demonstrating a strong agreement between predictions and desired results (see Supplementary Material: Inverse Design and Homogenization for more details).

Finally, in Figure 5(b), we apply our new numerical method to predict wrinkling in bilayers with different microstructural patterns. For this analysis, we design film layers with orthogonal oval, rectangular, and sinusoidal voids, each tailored to yield specific Poisson's ratios shown in Figure 5(b). The critical stretch ratio for buckling in bilayers with microstructural patterns aligns well with the homogenized model outcomes presented in Figure 3(d). Indeed, the relative error for the critical stretch between microstructural and the homogenized models is within 6.3%.

In conclusion, in this letter we investigated the possibility of harnessing wrinkles parallel to the direction of applied tension in 3D isotropic compressible bilayers subject to large elongations. We paid particular attention to the cases when the substrate is quasi-incompressible and when the film is highly auxetic. We used a semi-analytical approach to predict the onset of wrinkling. We wrote a new UHYPER subroutine for Blatz–Ko material models and new user-defined Python scripts to simulate wrinkling in compressible bilayers with periodic boundary conditions. These scripts can be used to perform a linear buckling analysis in Finite Element simulations with ABAQUS. For compressible

neo-Hookean bilayer systems, we derived asymptotic expressions for critical stretch ratio and critical wavenumber, which can be used under finite strains to determine the Young modulus of the film layer for buckling-based metrology applications. We found that wrinkles can be obtained only when the Poisson ratio of the substrate is greater than that of the film. When the Poisson ratios of film and substrate converge to a common value, the critical stretch ratio shoots up sharply and the wavelength of wrinkles is high. In the limit, the wrinkles are not present because there are no compressive stresses developing when the lateral expansions are the same for the film and substrate. Through multiple simulations we showed that by varying the material properties, we can harness or delay the onset of wrinkles.

Additionally, using inverse analysis, we designed film microstructures to achieve desired effective Poisson's ratios, validated with Finite Element code, FEAP. The critical stretch ratio for buckling in auxetic structures with microstructural patterns closely aligns with predictions from homogenized models.

Some of the limitations of our work include the consideration of isotropic strain energy function for auxetic structures, and deformation-independent effective material properties. Functional-grading of auxetics could also be explored with the methods presented in this study, see some preliminary works on harnessing instabilities in functionally-graded auxetic materials using tension-field theory [45, 46] and their applications [47–49].

Ultimately, the method developed in this letter could play a critical role in the manufacturing and testing of auxetic hydrogel organ patches [9] and skin grafts [50]. This approach could specifically guide the design of graft microstructures to prevent undesired wrinkling.

Acknowledgments



This project has received funding from the European Union's Horizon 2020 research and innovation programme under the Marie Skłodowska-Curie Grant Agreement No. 956401.

-
- [1] S. Timoshenko, *History of Strength of Materials: With a Brief Account of the History of Theory of Elasticity and Theory of Structures* (Dover Publications, New York, 1983).
 - [2] S. Mueller, B. Kruck, and P. Baudisch, Laserorigami: Laser-cutting 3d objects, in *Proceedings of the SIGCHI Conference on Human Factors in Computing Systems, CHI '13* (Association for Computing Machinery, New York, NY, USA, 2013) p. 2585–2592.
 - [3] S. Sun, M. Brandt, and M. Easton, Powder bed fusion processes: An overview, *Laser Additive Manufacturing*, 55 (2017).
 - [4] M. Y. Popereka and V. Balagurov, Ferromagnetic films having a negative Poisson ratio, *Soviet Physics, Solid state* **11**, 2938 (1970).
 - [5] F. Milstein and K. Huang, Existence of a negative Poisson ratio in fcc crystals, *Physical Review B* **19**, 2030 (1979).
 - [6] R. Lakes, *Advances in negative Poisson's ratio materials* (1993).
 - [7] W. J. S. Dolla, B. A. Fricke, and B. R. Becker, Structural and Drug Diffusion Models of Conventional and Auxetic Drug-Eluting Stents, *Journal of Medical Devices* **1**, 47 (2006).
 - [8] A. Lazarus and P. M. Reis, Soft actuation of structured cylinders through auxetic behavior, *Advanced Engineering Materials* **17**, 815 (2015).
 - [9] P. Chansoria, J. Blackwell, E. L. Etter, E. E. Bonacquisti, N. Jasiewicz, T. Neal, S. A. Kamal, J. Hoque, S. Varghese, T. Egan, and J. Nguyen, Rationally designed anisotropic and auxetic hydrogel patches for adaptation to dynamic organs, *Advanced Functional Materials* **32**, 2207590 (2022).
 - [10] N. Bowden, S. Brittain, A. G. Evans, J. W. Hutchinson, and G. M. Whitesides, Spontaneous formation of ordered structures in thin films of metals supported on an elastomeric polymer, *Nature* **393**, 146 (1998).
 - [11] S. Wagner, S. P. Lacour, J. Jones, P. hui I. Hsu, J. C. Sturm, T. Li, and Z. Suo, Electronic skin: architecture and components, *Physica E: Low-dimensional Systems and Nanostructures* **25**, 326 (2004), proceedings of the 13th International Winterschool on New Developments in Solid State Physics - Low-Dimensional Systems.
 - [12] D.-Y. Khang, H. Jiang, Y. Huang, and J. A. Rogers, A stretchable form of single-crystal silicon for high-performance electronics on rubber substrates, *Science* **311**, 208 (2006).
 - [13] J. Zhang, Y. Li, and Y. Xing, Theoretical and experimental investigations of transient thermo-mechanical analysis on flexible electronic devices, *International Journal of Mechanical Sciences* **160**, 192 (2019).
 - [14] C. Harrison, C. M. Stafford, W. Zhang, and A. Karim, Sinusoidal phase grating created by a tunably buckled surface, *Applied Physics Letters* **85**, 4016 (2004).
 - [15] C. M. Stafford, C. Harrison, K. L. Beers, A. Karim, E. J. Amis, M. R. VanLandingham, H.-C. Kim, W. Volksen, R. D. Miller, and E. E. Simonyi, A buckling-based metrology for measuring the elastic moduli of polymeric thin films, *Nature Materials* **3**, 545 (2004).
 - [16] J. Huang, M. Juskiewicz, W. H. de Jeu, E. Cerda, T. Emrick, N. Menon, and T. P. Russell, Capillary wrinkling of floating thin polymer films, *Science* **317**, 650 (2007).
 - [17] P.-C. Lin and S. Yang, Mechanically switchable wetting on wrinkled elastomers with dual-scale roughness, *Soft Matter* **5**, 1011 (2009).
 - [18] A. J. Crosby, Why should we care about buckling?, *Soft Matter* **6**, 5660 (2010).
 - [19] A. L. Volynskii, S. Bazhenov, O. V. Lebedeva, and N. F. Bakeev, Mechanical buckling instability of thin coatings deposited on soft polymer substrates, *Journal of Materials Science* **35**, 547 (2000).
 - [20] Z. Cai and Y. Fu, On the imperfection sensitivity of a coated elastic half-space, *Proceedings of the Royal Society of London. Series A: Mathematical, Physical and Engineering Sciences* **455**, 3285 (1999).
 - [21] K. Efimenko, M. Rackaitis, E. Manias, A. Vaziri, L. Mahadevan, and J. Genzer, Nested self-similar wrinkling patterns in skins, *Nature Materials* **4**, 293 (2005).
 - [22] A. Goriely and M. Ben Amar, Differential growth and instability in elastic shells, *Phys. Rev. Lett.* **94**, 198103 (2005).
 - [23] C. M. Stafford, S. Guo, C. Harrison, and M. Y. M. Chiang, Combinatorial and high-throughput measurements of the modulus of thin polymer films, *Review of Scientific Instruments* **76**, 062207 (2005).
 - [24] H. Li, S. Cai, Y. Zhang, K.-C. Hwang, Y. Ma, and X. Feng, Local wrinkling versus global buckling of stiff film bonded to finite-thick substrate, *Extreme Mechanics Letters* **29**, 100453 (2019).
 - [25] Y. Cao and J. W. Hutchinson, From wrinkles to

- creases in elastomers: the instability and imperfection-sensitivity of wrinkling, *Proceedings of the Royal Society A: Mathematical, Physical and Engineering Sciences* **468**, 94 (2012).
- [26] F. Brau, P. Damman, H. Diamant, and T. A. Witten, Wrinkle to fold transition: influence of the substrate response, *Soft Matter* **9**, 8177 (2013).
- [27] L. Zhuo and Y. Zhang, From period-doubling to folding in stiff film/soft substrate system: The role of substrate nonlinearity, *International Journal of Non-Linear Mechanics* **76**, 1 (2015).
- [28] D. Bigoni, N. Bordignon, A. Piccolroaz, and S. Stupkiewicz, Bifurcation of elastic solids with sliding interfaces, *Proceedings of the Royal Society A: Mathematical, Physical and Engineering Sciences* **474**, 20170681 (2018).
- [29] A. D. Bakiler and A. Javili, Understanding the role of interfacial mechanics on the wrinkling behavior of compressible bilayer structures under large plane deformations, *Mathematics and Mechanics of Solids* **28**, 748 (2023).
- [30] S. Nikraves, D. Ryu, and Y.-L. Shen, Surface instability of composite thin films on compliant substrates: Direct simulation approach, *Frontiers in Materials* **6**, 10.3389/fmats.2019.00214 (2019).
- [31] ABAQUS Inc., *ABAQUS/Standard User's Manual, Version 2019* (Dassault Systèmes Simulia Corp, United States, 2019).
- [32] P. J. Blatz and W. L. Ko, Application of finite elastic theory to the deformation of rubbery materials, *Transactions of the Society of Rheology* **6**, 223 (1962).
- [33] J. Crespo and F. J. Montáns, A continuum approach for the large strain finite element analysis of auxetic materials, *International Journal of Mechanical Sciences* **135**, 441 (2018).
- [34] A. Bonfanti and A. Bhaskar, Elastic stabilization of wrinkles in thin films by auxetic microstructure, *Extreme Mechanics Letters* **33**, 100556 (2019).
- [35] J. Ciambella and G. Saccomandi, A continuum hyperelastic model for auxetic materials, *Proceedings of the Royal Society A: Mathematical, Physical and Engineering Sciences* **470**, 20130691 (2014).
- [36] J. B. Choi and R. S. Lakes, Non-linear properties of metallic cellular materials with a negative poisson's ratio, *Journal of Materials Science* **27**, 5375 (1992).
- [37] S. Nikraves, D. Ryu, and Y.-L. Shen, Direct numerical simulation of buckling instability of thin films on a compliant substrate, *Advances in Mechanical Engineering* **11**, 1687814019840470 (2019).
- [38] Wolfram Research Inc., *Mathematica*, Version 13.1, Champaign, IL (2022).
- [39] J. Y. Chung, A. J. Nolte, and C. M. Stafford, Surface wrinkling: A versatile platform for measuring thin-film properties, *Advanced Materials* **23**, 349 (2011).
- [40] Z. Cai and Y. Fu, Exact and asymptotic stability analyses of a coated elastic half-space, *International Journal of Solids and Structures* **37**, 3101 (2000).
- [41] Z. Cai and Y. Fu, Effects of pre-stretch, compressibility and material constitution on the period-doubling secondary bifurcation of a film/substrate bilayer, *International Journal of Non-Linear Mechanics* **115**, 11 (2019).
- [42] K. Bertoldi, V. Vitelli, J. Christensen, and M. Van Hecke, Flexible mechanical metamaterials, *Nature Reviews Materials* **2**, 1 (2017).
- [43] H. Danesh, D. Di Lorenzo, F. Chinesta, S. Reese, and T. Brepols, Fft-based surrogate modeling of auxetic metamaterials with real-time prediction of effective elastic properties and swift inverse design, *arXiv preprint arXiv:2408.13532* (2024).
- [44] R. L. Taylor, *Feap-a finite element analysis program* (2014).
- [45] S. P. Venkata, V. Balbi, M. Destrade, D. Accoto, and G. Zurlo, Programmable wrinkling for functionally-graded auxetic circular membranes, *Extreme Mechanics Letters* **63**, 102045 (2023).
- [46] S. Pamulaparthy Venkata, V. Balbi, M. Destrade, and G. Zurlo, Designing necks and wrinkles in inflated auxetic membranes, *International Journal of Mechanical Sciences* **268**, 109031 (2024).
- [47] Q. Zhao, J. Wang, H. Cui, H. Chen, Y. Wang, and X. Du, Programmed shape-morphing scaffolds enabling facile 3d endothelialization, *Advanced Functional Materials* **28**, 1801027 (2018).
- [48] Y. Zahoor, R. De Breucker, and M. Voskuil, Preliminary design of a te morphing surface for rotorcraft, in *AIAA Scitech 2020 Forum* (2020) p. 1301.
- [49] J. Babič, M. Laffranchi, F. Tessari, T. Verstraten, D. Novak, N. Šarabon, B. Ugurlu, L. Peternel, D. Torricelli, and J. F. Veneman, Challenges and solutions for application and wider adoption of wearable robots, *Wearable Technologies* **2**, e14 (2021).
- [50] V. Gupta and A. Chanda, Biomechanical modelling of hierarchical metamaterials for skin grafting, in *Materials for Biomedical Simulation: Design, Development and Characterization* (Springer Nature Singapore, Singapore, 2023) pp. 71–83.

Supplementary material: Wrinkling of 3D auxetic bilayers in tension

Sairam Pamulaparthy Venkata^{*,†}, Valentina Balbi, and Michel Destrade
*School of Mathematical and Statistical Sciences,
 University of Galway, H91 TK33 Galway, Ireland*

Yuxin Fu[†]
*Department of Mechanics,
 Tianjin University, Tianjin 300072, China*

Hooman Danesh
*Institute of Applied Mechanics,
 RWTH Aachen University,
 Mies-van-der-Rohe-Str.1, 52074, Aachen, Germany*

Yibin Fu
*School of Computer Science and Mathematics,
 Keele University, Keele,
 Staffordshire ST5 5BG, United Kingdom*

** Contact author: S.PamulaparthyVenkata1@universityofgalway.ie*

† These authors contributed equally to this work.

SEMI-ANALYTICAL METHOD

To calculate the critical stretch and wavelength of the wrinkling instability, we use the small-on-large method. We first calculate the base (elastic) solution, we then superimpose an incremental deformation and derive the equations of the associated incremental problem.

We use the Blatz-Ko model (Equation (1) in the main manuscript) and calculate the principal components of the Cauchy stress $\mathbf{T} = J^{-1}\mathbf{F}(\partial W/\partial \mathbf{F})$ as

$$T_i = E \frac{J^{-(2\alpha+1)} (-\alpha\lambda_i^2 + (\alpha-1 + \alpha\lambda_i^4)J^{2\alpha} - (\alpha-1)\lambda_i^2 J^{4\alpha})}{2\lambda_i^2(1+\nu)}, \quad (\text{S.1})$$

where the λ_i are the principal stretch ratios and $J = \det \mathbf{F}$.

The substrate is under uniaxial tension along X, so that $T_{22}^s = T_{33}^s = 0$, which gives the following deformation gradient,

$$\mathbf{F}^s = \text{diag} (\lambda_1, \lambda_1^{-\nu_s}, \lambda_1^{-\nu_s}). \quad (\text{S.2})$$

The film and substrate are perfectly bonded, so that $\lambda_1^f = \lambda_1^s$, $\lambda_3^f = \lambda_3^s$, and $T_{22}^f = T_{22}^s = 0$. We then find that

$$\mathbf{F}^f = \text{diag} \left(\lambda_1, \lambda_1^{\frac{\nu_f(\nu_s-1)}{(1-\nu_f)}}, \lambda_1^{-\nu_s} \right). \quad (\text{S.3})$$

Equations (S.2), (S.3) together with (S.1) define the base state (elastic solution) of the bilayer in tension.

To find the critical state of buckling, we superimpose a small-amplitude displacement \mathbf{u} on the finite deformations in Equations (S.2) and (S.3). By following Ogden [1], we obtain the following incremental equations of equilibrium:

$$\begin{aligned} \mathcal{A}_{0jilm}^s u_{m,lj}^s &= 0, & -\infty < y < 0, \\ \mathcal{A}_{0jilm}^f u_{m,lj}^f &= 0, & 0 < y < h, \end{aligned} \quad (\text{S.4})$$

where the commas denote differentiation with respect to the coordinates, h is the current thickness of the film, and \mathcal{A}_0 is the fourth-order tensor of the instantaneous elastic moduli, with components

$$\mathcal{A}_{0jilm} = J^{-1} F_{j\alpha} \frac{\partial^2 W}{\partial F_{i\alpha} \partial F_{m\beta}} F_{l\beta}. \quad (\text{S.5})$$

We look for solutions of the forms:

$$u_z = e^{sy} \sin(kz), \quad u_y = e^{sy} \cos(kz), \quad (\text{S.6})$$

where s is the attenuation coefficient and k is the wavenumber of the sinusoidal wrinkles. Substitution into Equation (S.4) leads to an eigenproblem, with characteristic equation a bicubic in s . In the film, the general solution is of the form

$$u_z^f = \left(\sum_{i=1}^4 \mathcal{V}_i e^{s_i y} \right) \sin(kz), \quad u_y^f = \left(\sum_{i=1}^4 \mathcal{V}_i e^{s_i y} \right) \cos(kz), \quad (\text{S.7})$$

where s_1, \dots, s_4 are the eigenvalues, and $\mathcal{V}_1, \dots, \mathcal{V}_4$ are constants. In the substrate, the stretch ratios along the Y- and Z- directions are equal, and $s = 1$ is a repeated eigenvalue. The other repeated root, $s = -1$ is discarded to enforce decay. There, the solution is thus of the form

$$u_z^s = (\mathcal{U}_1 + \mathcal{U}_2 y) e^y \sin(kz), \quad u_y^s = (\mathcal{U}_1 + \mathcal{U}_2 y) e^y \cos(kz), \quad (\text{S.8})$$

where $\mathcal{U}_1, \mathcal{U}_2$ are constants.

By applying the traction-free boundary conditions

$$\mathcal{A}_{02ilm}^f u_{m,l}^f = 0, \quad y = h, \quad (\text{S.9a})$$

and the continuity conditions

$$\mathcal{A}_{02ilm}^f u_{m,l}^f = \mathcal{A}_{02ilm}^s u_{m,l}^s, \quad u_i^f = u_i^s, \quad y = 0, \quad (\text{S.9b})$$

we obtain six homogeneous equations for $\{\mathcal{U}_1, \mathcal{U}_2, \mathcal{V}_1, \dots, \mathcal{V}_4\}$. The bifurcation condition is then given by equating the determinant of a 6×6 coefficient matrix to 0.

FINITE ELEMENT SIMULATIONS

We first checked the accuracy of our periodic boundary conditions (PBCs) python code to reproduce known results for wrinkling under plane-strain compression. Hence, we performed a linear buckling analysis in ABAQUS on an incompressible neo-Hookean 2D bilayer periodic along the X-direction and recovered the results of Cao and Hutchinson [2]. Our model is shown in Figure S.1(a) and the benchmark results in Figure S.1(b).

We then perform a series of finite-element simulations for 3D Blatz-Ko bilayers under uni-axial tension. The dimensions (X, Y, Z) of the bilayer are $15 \times 45 \times 5.684$ units with $h_s/h_f = 299$ when the substrate is incompressible, and $15 \times 80 \times 4.504$ units with $h_s/h_f = 399$ when the film is highly auxetic. Here, h_s and h_f are the thickness of the film and substrate, respectively.

The dimensions along the Z-direction are integer multiples of the wavelength (calculated using semi-analytical results from Mathematica).

We apply PBCs on the lateral faces in the X- and Z-directions of the domain.

Both the film and substrate are modelled using a UHYPER subroutine with the Blatz-Ko strain energy function. We use a 20-node brick (hexahedral) element with quadratic interpolation and reduced integration (C3D20R) for both film and substrate; for the incompressible case, we used a C3D20RH element. For the Blatz-Ko bilayers, 34,200 and 17,130 mesh elements are used for the cases of incompressible substrate and highly auxetic film, respectively. For the neo-Hookean bilayer, 3,240 mesh elements are used.

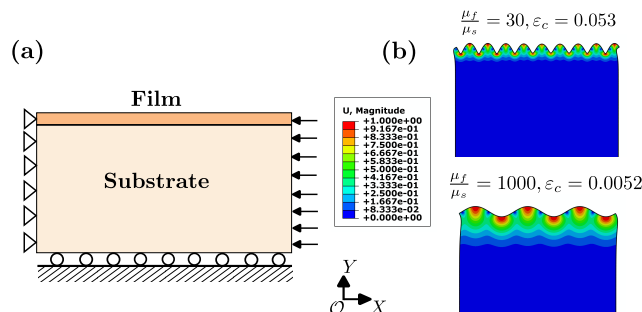


Figure S.1. (a) Schematic representation of an incompressible neo-Hookean stiff film/soft substrate bilayer system under uni-axial compression. On the left edge of the domain, displacement and shear traction are set at zero. On the bottom edge of the domain, roller support restricts vertical displacement and shear traction, and the top surface of the film is traction-free. (b) Linear buckling solutions with critical strains ϵ_c when $\mu_f/\mu_s = 30, 1000$, in line with the predictions of Cao and Hutchinson [2].

ASYMPTOTIC ANALYSIS

In Volynskii *et al.* [3], Chung *et al.* [4], and Nikravesh *et al.* [5], the authors derive the following critical strain and wavenumber expressions:

$$\varepsilon_c = \frac{1}{4(\nu_s - \nu_f)} \left(3 \frac{\mu_s}{\mu_f} \frac{1 - \nu_f}{1 - \nu_s} \right)^{2/3} \quad \text{and} \quad k_c h = \left(3 \frac{\mu_s}{\mu_f} \frac{1 - \nu_f}{1 - \nu_s} \right)^{1/3}, \quad (\text{S.10})$$

for linearly elastic bilayers under uniaxial tension. These expressions are valid under the plane-strain approximation. Here, h is the current thickness of the film, ε_c is the critical strain, and k_c is the critical wavenumber. Equation (S.10) is used in the plots of Figure 4 in the main manuscript.

However, we note that the plane-strain assumption is not valid for a bilayer system under uni-axial tension. Here, we follow Cai and Fu [6, 7] and assume that the shear modulus ratio $r = \mu_s/\mu_f$ is of order $(k_c h)^3$ to derive asymptotic expansions for the critical strain and wavenumber (for simplicity, we take $\alpha_s = \alpha_f = 1$ in Equation (1) in the main manuscript).

To derive the asymptotic expressions, we assume the following ansatz:

$$k_c h = \sum_{i=1}^5 d_i \delta^i + \mathcal{O}(\delta^6), \quad \lambda_c = 1 + \sum_{\substack{j=1 \\ j \neq 2}}^6 c_j \delta^j + \mathcal{O}(\delta^7), \quad \delta = \left(\frac{\mu_s}{\mu_f} \right)^{1/3}. \quad (\text{S.11})$$

From Equation (S.3), the component F_{22} of the film layer can be expressed as a series expansion in terms of δ as follows:

$$F_{22}^f = \lambda_1^{\frac{\nu_f(\nu_s-1)}{(1-\nu_f)}} = 1 + \sum_{i=1}^8 \hat{d}_i \delta^i + \mathcal{O}(\delta^9). \quad (\text{S.12})$$

Similarly, the attenuation coefficients for the film layer s_1, \dots, s_4 and their squares can be expressed as a series expansion in terms of δ upto 8 terms. These simplifications will help in reducing the computational time.

Finally, the expressions for the attenuation coefficients (s_1, \dots, s_4), $k_c h$, λ_c , and F_{22}^f in terms of δ are substituted into the bifurcation equation and its derivative with respect to $k_c h$. This process results in the bifurcation equation and its derivative being represented as series expansions in δ , up to 12 and 11 terms respectively, while higher-order terms are ignored.

We observe that by equating the coefficients of δ^i and δ^{i-1} in the bifurcation equation and its derivative with respect to $k_c h$ (for all $i \geq 8$) to zero simultaneously, we can determine the parameters c_{j+1} and d_j for $j \geq 1$, respectively.

Using this procedure, we obtain

$$\lambda_c = 1 + \frac{[(1 - \nu_f)(1 - \nu_s)]^{2/3}}{(\nu_s - \nu_f)(8\nu_s/3 - 2)^{2/3}} r^{2/3} + \frac{(1 - \nu_f)(2\nu_s - 1)}{(\nu_s - \nu_f)(4\nu_s - 3)} r + c_4 r^{4/3} + c_5 r^{5/3} + c_6 r^2 + \mathcal{O}(r^{7/3}), \quad (\text{S.13})$$

and

$$k_c h = \left[\frac{4(1 - \nu_f)(1 - \nu_s)}{1 - 4\nu_s/3} \right]^{1/3} r^{1/3} + d_3 r + d_4 r^{4/3} + d_5 r^{5/3} + \mathcal{O}(r^2), \quad (\text{S.14})$$

where the coefficients $c_4, \dots, c_6, d_3, \dots, d_5$ are given by the following expressions:

$$c_4 = \frac{\mathcal{C} \left(45 + \nu_s c_{4a} + \nu_f c_{4b} + \nu_f^2 c_{4c} \right)}{20 \times 2^{1/3} \times 3^{2/3} (\nu_f - \nu_s)^2 (-1 + \nu_s) (-3 + 4\nu_s)^{4/3}}, \quad c_5 = \frac{\mathcal{C}^2 (-1 + \nu_f) (-1 + 2\nu_s) (-3 - 4\nu_f + 4\nu_s)}{22^{2/3} \times 3^{1/3} (\nu_f - \nu_s)^2 (-3 + 4\nu_s)^{5/3}}, \quad (\text{S.15a})$$

$$c_6 = \frac{4725 - 2\nu_f^4 c_{6a} - \nu_s c_{6b} + \nu_f^3 c_{6c} + \nu_f^2 c_{6d} + 2\nu_f c_{6e}}{12600(3 - 4\nu_s)^2 (-1 + \nu_s)^2 (-\nu_f + \nu_s)^3}, \quad \mathcal{C} = ((1 - \nu_f)(\nu_s - 1))^{1/3},$$

and

$$\begin{aligned} c_{4a} &= -64 + (13 - 4\nu_s)\nu_s, & c_{4b} &= -71 + \nu_s(66 + (51 - 26\nu_s)\nu_s), & c_{4c} &= 56 - 92\nu_s + 26\nu_s^2, \\ c_{6a} &= 33727 + 2\nu_s(-73474 + \nu_s(122601 + \nu_s(-92584 + 26681\nu_s))), \\ c_{6b} &= 4410 + \nu_s(82574 + \nu_s(-288226 + \nu_s(399999 - 260716\nu_s + 67034\nu_s^2))), \\ c_{6c} &= 95848 + 2\nu_s(-138872 + \nu_s(46253 + \nu_s(235988 + \nu_s(-297317 + 106724\nu_s))), \\ c_{6d} &= -3509 + \nu_s(-202720 + \nu_s(841376 + \nu_s(-1218634 + \nu_s(643241 + 2(22435 - 53362\nu_s)\nu_s))), \\ c_{6e} &= -11970 + \nu_s(78479 + \nu_s(-137927 + \nu_s(-12652 + \nu_s(271583 + \nu_s(-276527 + 89714\nu_s))))). \end{aligned} \quad (\text{S.15b})$$

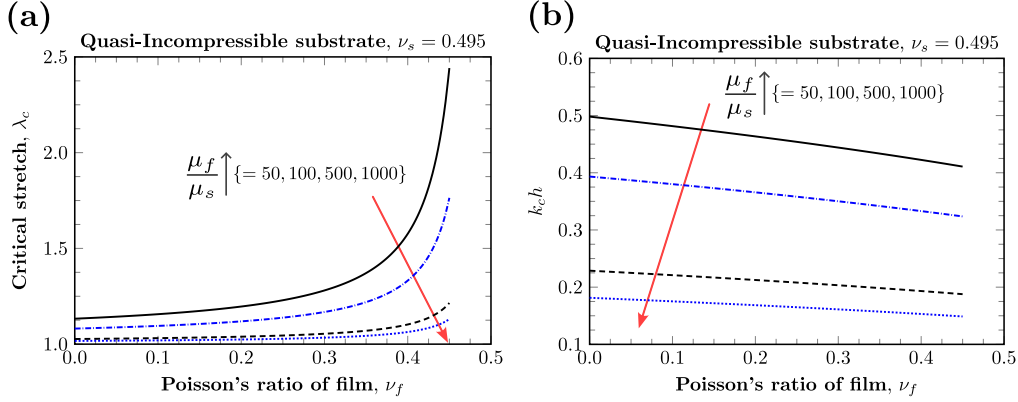


Figure S.2. Using the asymptotic expressions in Equations S.13-S.14 for compressible neo-Hookean materials ($\alpha_s = \alpha_f = 1$ in Equation 1, main manuscript). The substrate is quasi-incompressible ($\nu_s = 0.495$). (a-b): Variations of the critical stretch of wrinkling λ_c and corresponding critical wavenumber measure $k_c h$ with the Poisson ratio of film layer (k_c is the critical wavenumber and h is the deformed film thickness) and for contrast in shear moduli between the layers ($\mu_f/\mu_s = \{50, 100, 500, 1000\}$).

Similarly, the coefficients of higher-order terms in the asymptotic expression for critical wavenumber (Equation (S.14)) are

$$d_3 = \frac{4 + 2\nu_s - 11\nu_s^2 + \nu_f(11 - 32\nu_s + 26\nu_s^2)}{15(3 - 7\nu_s + 4\nu_s^2)}, \quad d_4 = \frac{\left(\frac{2}{3}\right)^{2/3} \mathcal{C}(1 + 2\nu_f)(-1 + 2\nu_s)}{(-3 + 4\nu_s)^{4/3}}, \quad (\text{S.16a})$$

$$d_5 = \frac{\mathcal{C}^2(-6761 + \nu_s d_{5a} + 4\nu_f^2 d_{5b} - 2\nu_f d_{5c})}{3150 \times 2^{2/3} \times 3^{1/3} (-1 + \nu_f)(-1 + \nu_s)^3 (-3 + 4\nu_s)^{5/3}},$$

and

$$\begin{aligned} d_{5a} &= 21724 + \nu_s(-19146 + \nu_s(-2636 + 7519\nu_s)), \\ d_{5b} &= 646 + \nu_s(-4964 + \nu_s(12906 + \nu_s(-14204 + 5791\nu_s))), \\ d_{5c} &= -3821 + \nu_s(7864 + \nu_s(5844 + \nu_s(-22796 + 13609\nu_s))). \end{aligned} \quad (\text{S.16b})$$

In Figure S.2(a-b), we plot the variations of λ_c and $k_c h$ with the Poisson ratio of the film ($0 < \nu_f < 0.45$) for different values of shear moduli contrast μ_f/μ_s using Equations S.13-S.14, because they give curves instantly compared to ABAQUS simulations. We recall our assumption that r is in the order of $(k_c h)^3$, therefore when μ_f/μ_s increases or r decreases, we obtain low values of critical wavenumber and long wavelength wrinkles, see Figure S.2(b). For an incompressible neo-Hookean substrate, the wavelength of wrinkles increases as the Poisson's ratios of the film and substrate approach each other, as shown in Figure S.2(b).

INVERSE DESIGN AND HOMOGENIZATION

Building on the surrogate models developed by Danesh *et al.* [8] for orthogonal void auxetic structures in the small strain regime, an inverse design approach was employed to efficiently determine the geometric parameters of a chosen auxetic unit cell. This method precisely tailors the unit cell to achieve specific components of effective elastic stiffness based on the material properties of the base constituent. By employing Voigt notation, Danesh *et al.* [8] demonstrated that the in-plane effective stress of these orthogonal void auxetic unit cells can be directly correlated with their effective strain through the components of the effective stiffness as

$$\begin{pmatrix} \overline{T}_{11} \\ \overline{T}_{22} \\ \overline{T}_{12} \end{pmatrix} = \begin{pmatrix} \overline{C}_{11} & \overline{C}_{12} & 0 \\ \overline{C}_{12} & \overline{C}_{11} & 0 \\ 0 & 0 & \overline{C}_{33} \end{pmatrix} \begin{pmatrix} \overline{\varepsilon}_{11} \\ \overline{\varepsilon}_{22} \\ 2\overline{\varepsilon}_{12} \end{pmatrix}. \quad (\text{S.17})$$

Here, $\overline{(\bullet)}$ refers to the homogenized averaged value of a quantity, including stress, strain, and elastic stiffness components. Therefore, if we define the components of the effective stiffness \overline{C}_{11} and \overline{C}_{12} , we can obtain the desired effective Poisson's ratio $\nu_f^{\text{eff}} = \overline{C}_{12}/\overline{C}_{11}$. Considering a linear isotropic material with Young's modulus $E_f = 110$ GPa and Poisson's ratio $\nu_f = 0.1$, we employed the aforementioned inverse design approach to generate auxetic structures with desired effective Poisson's ratios $\nu_f^{\text{eff}} = -0.02, -0.18,$ and -0.48 , which were used for wrinkling analysis presented in Figure 5(b) of the main manuscript.

In order to validate the obtained geometries from the inverse design, we utilized the finite element code FEAP [9]. To do so, we discretized the unit cells with linear quadrilateral elements and performed homogenization to compute the effective elastic stiffness. We ensured the existence of symmetric nodes on the opposing boundaries and applied periodic boundary conditions. After computing the effective elastic stiffness of each unit cell, we verified that we could recover the desired effective Poisson's ratio with high precision.

-
- [1] D. Haughton and R. Ogden, On the incremental equations in non-linear elasticity— I. Membrane theory, *Journal of the Mechanics and Physics of Solids* **26**, 93 (1978).
 - [2] Y. Cao and J. W. Hutchinson, Wrinkling Phenomena in Neo-Hookean Film/Substrate Bilayers, *Journal of Applied Mechanics* **79**, 031019 (2012).
 - [3] A. L. Volynskii, S. Bazhenov, O. V. Lebedeva, and N. F. Bakeev, Mechanical buckling instability of thin coatings deposited on soft polymer substrates, *Journal of Materials Science* **35**, 547 (2000).
 - [4] J. Y. Chung, A. J. Nolte, and C. M. Stafford, Surface wrinkling: A versatile platform for measuring thin-film properties, *Advanced Materials* **23**, 349 (2011).
 - [5] S. Nikraves, D. Ryu, and Y.-L. Shen, Direct numerical simulation of buckling instability of thin films on a compliant substrate, *Advances in Mechanical Engineering* **11**, 1687814019840470 (2019).
 - [6] Z. Cai and Y. Fu, Exact and asymptotic stability analyses of a coated elastic half-space, *International Journal of Solids and Structures* **37**, 3101 (2000).
 - [7] Z. Cai and Y. Fu, Effects of pre-stretch, compressibility and material constitution on the period-doubling secondary bifurcation of a film/substrate bilayer, *International Journal of Non-Linear Mechanics* **115**, 11 (2019).
 - [8] H. Danesh, D. Di Lorenzo, F. Chinesta, S. Reese, and T. Brepols, Fft-based surrogate modeling of auxetic metamaterials with real-time prediction of effective elastic properties and swift inverse design, arXiv preprint arXiv:2408.13532 (2024).
 - [9] R. L. Taylor, Feap-a finite element analysis program (2014).